Interpreting Unary, Binary, and Ternary Mixture Permeation Across a SAPO-34 Membrane with Loading-Dependent Maxwell−Stefan Diffusivities

Shiguang Li,[†] John L. Falconer,[†] Richard D. Noble,[†] and R. Krishna*[,‡]

Department of Chemical and Biological Engineering, University of Colorado, Boulder, Colorado 80309-0424 and Van't Hoff Institute for Molecular Sciences, University of Amsterdam, Nieuwe Achtergracht 166, 1018 WV Amsterdam, The Netherlands

Received: November 9, 2006; In Final Form: January 5, 2007

Unary permeation experiments were performed with He, H_2, CO_2, N_2, O_2, CO, Ar, and CH_4 across a SAPO-34 membrane at 295 K with upstream pressures ranging to 7.2 MPa, ensuring that high occupancies within the zeolite layer are reached. Careful analysis of the unary permeation experiments shows that the Maxwell−Stefan (M-S) diffusivity $Đ_i$ is loading-dependent for all gases except He and H_2. The model of Reed and Ehrlich (*Surf. Sci.* **1981**, *102*, 588−609) was used to describe the loading-dependence of $Đ_i$. The zero-loading diffusivity $Đ_i(0)$ and the Reed−Ehrlich parameter ϕ_i are backed out from the permeation experiments, providing a complete description of $Đ_i$ as a function of loading, q_i. Permeation experiments for CO_2/CH_4, CO_2/N_2, N_2/CH_4, H_2/CH_4, H_2/N_2, H_2/CO, and $CO_2/CH_4/N_2$ mixtures were performed to determine to what extent loading-dependent M-S diffusivities influence permeation fluxes and selectivities. Good agreement between the M-S mixture model and experiments are obtained, provided the binary exchange coefficients $Đ_{ij}$ in the M-S uations are assumed to have high enough values to ensure that intercage hops of the molecules occur practically independently of one other.

1. Introduction

A proper description of diffusion of molecules within nanoporous materials such as zeolites, carbon nanotubes, and metal−organic frameworks is required in many potential separation and reaction applications.[1−5] The Maxwell−Stefan formulation for single component diffusion in zeolites is commonly expressed as

$$N_i = -\rho Đ_i \frac{q_i}{RT}\frac{d\mu_i}{dx} \text{ (pure component } i\text{)} \qquad (1)$$

where N_i is the molar flux expressed in mol m^{-2} s^{-1}, ρ is the zeolite framework density expressed in kg m^{-3}, q_i is the molar loading expressed in mol kg^{-1}, $d\mu_i/dx$ is the chemical potential gradient, R is the gas constant, T is the absolute temperature in K, and $Đ_i$ is the Maxwell−Stefan (M-S) diffusivity, or "corrected" diffusivity of species i. In several classic publications on the subject of diffusion in zeolites, it has been customary to assume that $Đ_i$ is independent of the loading q_i within the zeolite.[6] However, in recent years there has been increasing evidence, both from experiments[7−10] and from molecular dynamics (MD) simulations[11−16] that $Đ_i$ is generally a strong function of loading. For any given molecule, say CH_4, the $Đ_i-q_i$ relation appears to be dependent both on the zeolite topology and connectivity.[11,17−20] For zeolites structures consisting of cages separated by narrow windows, such as LTA, CHA, ERI, and DDR, the $Đ_i$ increases sharply with loading q_i, reaches a maximum, and eventually decreases to near-zero values as the saturation loading $q_{i,sat}$ is approached.[13,17,18,21] The loading-dependence in such structures has been interpreted in terms of a reduction in the free energy barrier for intercage hopping with increased intracage occupancy.[18] The approach of Reed and Ehrlich[22] has been applied to cage-type zeolite structures to yield a simple analytical model to describe the dependence of $Đ_i$ on fractional occupancy θ_i, defined as

$$\theta_i = \frac{q_i}{q_{i,sat}} \qquad (2)$$

The primary objective of this paper is to investigate the loading-dependence of $Đ_i$ in a $(Si_{0.061}Al_{0.483}P_{0.455})O_2$ (SAPO-34) (an isotype of CHA) membrane by carrying out unary permeation experiments with a variety of light gases (He, H_2, CO_2, N_2, O_2, CO, Ar, and CH_4). For this purpose, experiments in an improved membrane were performed with upstream pressures ranging to 7.2 MPa to ensure high occupancies in the membrane. The membrane synthesis procedure used in the present study used a seeding procedure that resulted in a thinner membrane and higher fluxes than obtained in a previous study.[23] The details of membrane synthesis, characterization, measurement procedures along with the experimental data have been given in the Supporting Information. The current work supplements the unary permeation data for CO_2, N_2, and CH_4 reported in our earlier publication.[24]

In our earlier publication,[24] we had analyzed experimental data on permeation of binary mixtures CO_2/CH_4, CO_2/N_2, and CH_4/N_2 and concluded that for modeling purposes, the binary exchange coefficient $Đ_{12}$ in the M-S formulation is best taken to have a large enough value to ensure that intercage jumps of molecules occur independently of one another. In the current work, we report additional binary permeation data for H_2/CH_4, H_2/N_2, and H_2/CO mixtures to examine whether the conclusion reached in the earlier paper on independent intercage hopping

* To whom correspondence should be addressed. E-mail address: r.krishna@uva.nl. Fax: + 31 20 5255604.
[†] University of Colorado.
[‡] University of Amsterdam.

10.1021/jp067404j CCC: $37.00
Published on Web 03/13/2007

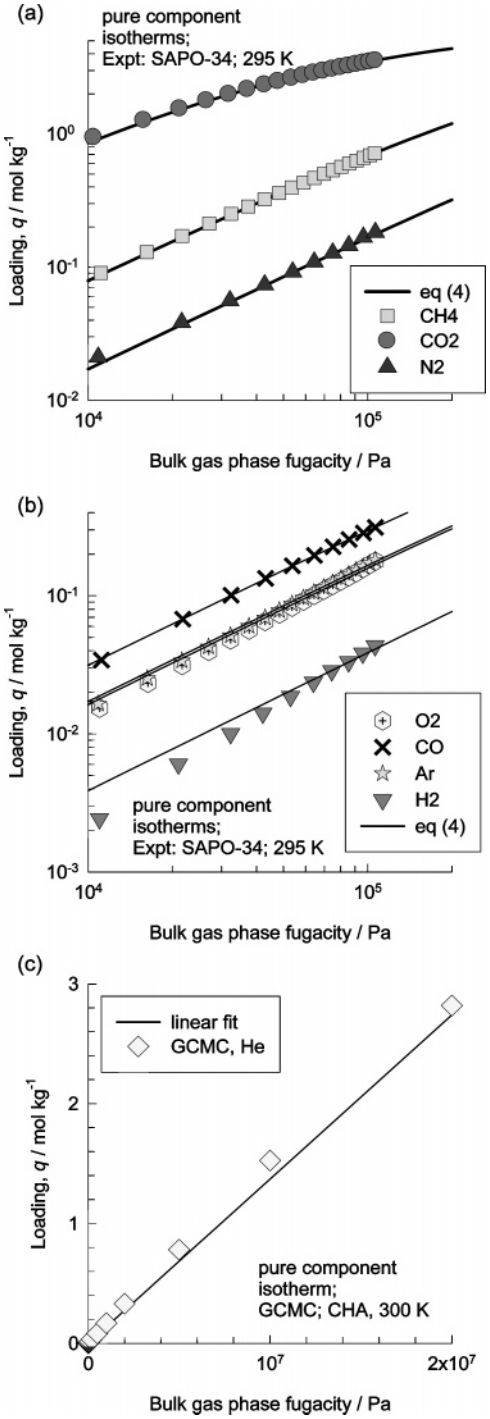

Figure 1. Pure component isotherm data for pure (a) CO_2, CH_4, N_2, (b) CO, Ar, O_2, H_2, and (c) He and along with fits using eq 3 or eq 5, denoted by the continuous solid lines. The He isotherm data is from GCMC simulations.

of molecules holds also for mixtures containing H_2. Furthermore, we report data for ternary $CO_2/CH_4/N_2$ mixture permeation experiments and examine whether the M-S formulation with infinite binary exchange coefficients $Đ_{ij}$ for each of the binary pairs is successful in predicting the permeation fluxes in the ternary mixture.

2. Fitting of Pure Component Isotherms

Adsorption experiments were carried out in an Autosorb-1 (Quantachrome Corp. Model AS1-C−VP-RGA) system. The experimental pure component isotherms for pure CO_2, CH_4, N_2, CO, Ar, O_2, and H_2 at 295 K are plotted in Figure 1a−c. For adsorption in zeolite structures with cages separated by narrow windows, such as SAPO-34, the model based on statistical thermodynamics described in Chapter 3 of Ruthven[25] is particularly relevant and useful.

TABLE 1: Pure Component Isotherm Fit Data Using Eq 3[a]

molecule	b_i	Ω_i	$q_{i,\mathrm{sat}}$
CO_2	7.67×10^{-5}	6	8.2
CH_4	5.87×10^{-6}	6	8.2
N_2	1.26×10^{-6}	6	8.2
H_2	2.84×10^{-7}	9	12.3
O_2	1.2×10^{-6}	6	8.2
CO	2.31×10^{-6}	6	8.2
Ar	1.26×10^{-6}	6	8.2

[a] b_i is expressed in Pa^{-1}, Ω_i is in molecules per cage, and $q_{i,\mathrm{sat}}$ is in mol kg^{-1}.

$$q_i = \frac{q_{i,\mathrm{sat}}}{\Omega_i} \frac{b_i f_i + \sum_{m=2}^{\Omega_i} \frac{(b_i f_i)^m}{(m-1)!} \left[\frac{1 - \frac{m}{\Omega_i + 1}}{1 - \frac{1}{\Omega_i + 1}}\right]^m}{1 + b_i f_i + \sum_{m=2}^{\Omega_i} \frac{(b_i f_i)^m}{(m)!} \left[\frac{1 - \frac{m}{\Omega_i + 1}}{1 - \frac{1}{\Omega_i + 1}}\right]^m} \quad (3)$$

In eq 3, q_i represents the loading in mol kg^{-1}, $q_{i,\mathrm{sat}}$ is the saturation loading, and Ω_i is maximum capacity expressed in molecules per cage. On the basis of the atomic composition of SAPO-34 used in our experiments, $(Si_{0.061}Al_{0.483}P_{0.455})O_2$, we calculate

$$q_{i,\mathrm{sat}} = 1.369\Omega_i \quad (4)$$

It is important to have a good estimate of the saturation capacity, $q_{i,\mathrm{sat}}$, but it is not possible to obtain this information from experimental isotherm data because the pressures at which the pores get saturated can range to about 10^9 Pa; our experimental isotherms were only determined to a maximum pressure of 110 kPa. For CO_2 for example, the molar volume of the liquid phase at 10^9 Pa is estimated to lie in the range of 30−35 cm^3/mol from the data given by Mäder and Berman.[26] Golden and Sircar[27] estimate the molar volumes for H_2, CO_2, N_2, Ar, and CH_4 to be 22.6, 33.3, 37.7, 26.3, and 31.6 cm^3/mol, respectively. Of these gases, CO_2 has the highest adsorption strength and the loading of CO_2 at the highest pressures used in the feed in the permeation experiments, to be discussed below, will be close to its saturation value. For the measured pore volume of 0.26 cm^3/g, the maximum capacity after rounding off to integer values is estimated to be 6 molecules per cage for CO_2, corresponding to 8.2 mol kg^{-1}. For H_2, using the value of 22.6 cm^3/mol for the molar volume results in a saturation capacity after rounding off of $\Omega_i = 9$ molecules per cage. Table 1 summarizes the values of the fit parameter b_i in eq 3.

For He, the measurement of the adsorption isotherm using the Autosorb-1 experimental setup was not feasible. In this case, we used Grand Canonical Monte Carlo (GCMC) simulations using the force field described in the literature[28] to determine the Henry coefficient H_i defined by

$$q_i = H_i f_i \quad \text{(Henry regime)} \tag{5}$$

The GCMC simulation data for all-silica CHA are presented in Figure 1c, and the best-fit value is $H_i = 1.37 \times 10^{-7}$ mol kg^{-1} Pa^{-1}; this value is assumed to be valid also for SAPO-34.

3. Analysis of Unary Permeation Data

If the M-S diffusivity $Đ_i$ can be taken to be loading-independent, we may write the permeation flux as

$$N_i = \frac{\rho Đ_i}{\delta} DF_i \tag{6}$$

where DF_i is the driving force

$$DF_i \equiv \int_{f_{i,\text{up}}}^{f_{i,\text{down}}} \frac{q_i}{f_i} \mathrm{d}f_i \tag{7}$$

where $f_{i,\text{up}}$ and $f_{i,\text{down}}$ represent the pressures (more strictly, fugacities) of component i at the upstream (retentate) and downstream (permeate) sides of the membrane. For He permeation, with eq 5 describing the adsorption isotherm in the Henry regime, the DF_i can be calculated from

$$DF_i = H_i (f_{i,\text{up}} - f_{i,\text{down}}) \tag{8}$$

For all other gases, the adsorption isotherms are described by eq 3 and the integral in eq 7 can be evaluated analytically to obtain

$$DF_i = \frac{q_{i,\text{sat}}}{\Omega_i} \ln \left(\frac{1 + b_i f_{i,\text{up}} + \sum_{m=2}^{\Omega_i} \frac{(b_i f_{i,\text{up}})^m}{(m)!} \left[\frac{1 - \frac{m}{\Omega_i + 1}}{1 - \frac{1}{\Omega_i + 1}} \right]^m}{1 + b_i f_{i,\text{down}} + \sum_{m=2}^{\Omega_i} \frac{(b_i f_{i,\text{down}})^m}{(m)!} \left[\frac{1 - \frac{m}{\Omega_i + 1}}{1 - \frac{1}{\Omega_i + 1}} \right]^m} \right) \tag{9}$$

Plots of the unary permeation fluxes for He and H_2 against the driving force DF_i are shown in Figure 2. The linear dependence of the flux N_i on DF_i confirms that the assumption of a loading-independent $Đ_i$ is a good one for He and H_2. The straight lines have been drawn taking the fitted value of $\rho Đ_i/\delta = 0.322$ and 0.293 kg m^{-2} s^{-1} for He and H_2, respectively.

The plots of N_i vs DF_i for CO_2, N_2, O_2, CO, Ar, and CH_4 are shown in Figure 3a,b. For none of these gases is the $N_i - DF_i$ relationship precisely linear. This is more clearly evident in Figure 4a,b in which the values of the transport coefficients, $\rho Đ_i/\delta$, backed out using eq 6, are plotted against the component loading at the upstream face of the membrane, $q_{i,\text{up}}$. For all gases, the $\rho Đ_i/\delta$ appears to increase with $q_{i,\text{up}}$. For CO_2, a slight maximum is also detectable at an upstream loading of 6 mol kg^{-1} beyond which the $\rho Đ_i/\delta$ appears to decrease with increasing $q_{i,\text{up}}$.

The values of transport coefficients $\rho Đ_i/\delta$ shown in Figure 4a,b do not reflect the true M-S diffusivities $Đ_i$ because they are based on eqs 6 and 7, which are derived assuming $Đ_i$ is independent of loading q_i. The proper procedure for backing out the M-S diffusivities is to first establish the correct $Đ_i - q_i$ dependence. To quantify the loading-dependence, we use the model developed by Reed and Ehrlich;[21,22,29] this model gives the following expression

$$Đ_i = Đ_i(0) \frac{(1 + \epsilon_i)^{z-1}}{(1 + \epsilon_i/\phi_i)^z} \tag{10}$$

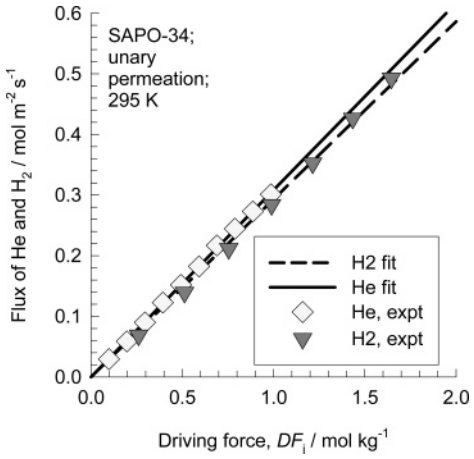

Figure 2. The experimental data on unary permeation fluxes for He and H_2 are plotted against the driving force DF_i, calculated from eq 8 for He or eq 9 for H_2. The straight lines have been drawn taking the fitted value of $\rho Đ_i/\delta = 0.322$ and 0.293 kg m^{-2} s^{-1} for He and H_2, respectively.

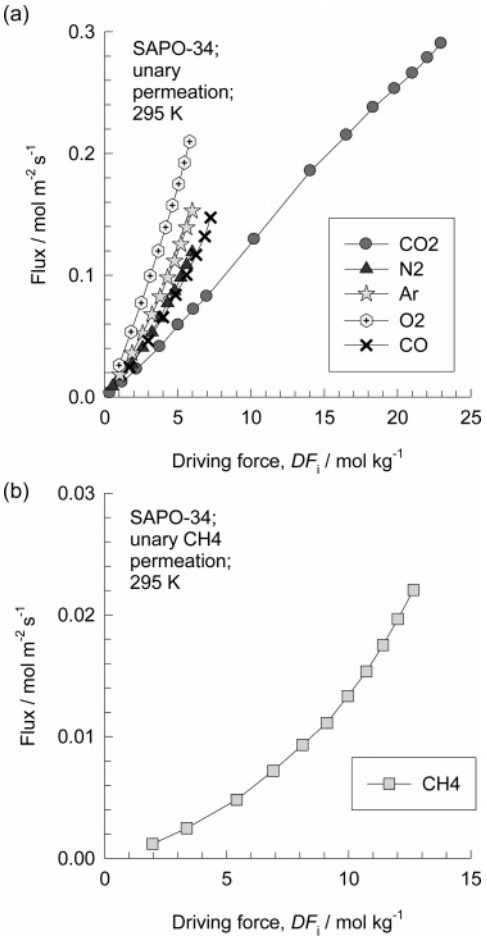

Figure 3. The plots of N_i vs DF_i for (a) CO_2, N_2, O_2, CO, Ar, and (b) CH_4.

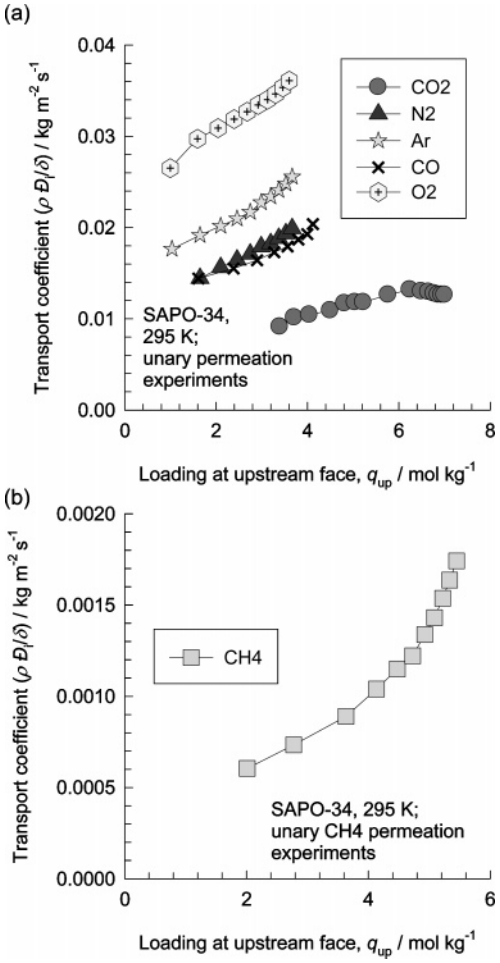

Figure 4. Transport coefficients $\rho Đ_i/\delta$ backed out using eq 6 (a) CO_2, N_2, O_2, CO, Ar, and (b) CH_4.

where z is the coordination number, representing the maximum number of neighbors within a cage; we take $z = 5$ (i.e., one less than the maximum capacity of molecules that can be accommodated in each cage). The other parameters are defined as (see Krishna et al.[21] for more detailed discussions and derivations)

$$\epsilon_i = \frac{(\beta_i - 1 + 2\theta_i)\phi_i}{2(1-\theta_i)}; \quad \beta_i = \sqrt{1 - 4\theta_i(1-\theta_i)(1-1/\phi_i)}; \quad \theta_i = \frac{q_i}{q_{i,\text{sat}}} \tag{11}$$

With the Reed−Ehrlich loading-dependence, we may define a modified driving force MDF_i

$$MDF_i \equiv \int_{f_{i,\text{down}}}^{f_{i,\text{up}}} \frac{(1+\epsilon_i)^{z-1}}{(1+\epsilon_i/\phi_i)^z} \frac{q_i}{f_i} \, \mathrm{d}f_i \tag{12}$$

The integration must be carried out numerically. The modified driving force must be expected to bear a linear relation with the permeation flux

$$N_i = \frac{\rho Đ_i(0)}{\delta} MDF_i \tag{13}$$

The plots for CO_2, N_2, CO, O_2, Ar, and CH_4 are shown in Figure 5a−c. The Reed−Ehrlich parameter ϕ_i was chosen to yield a straight line relationship; the best fit values of ϕ_i that yield linear

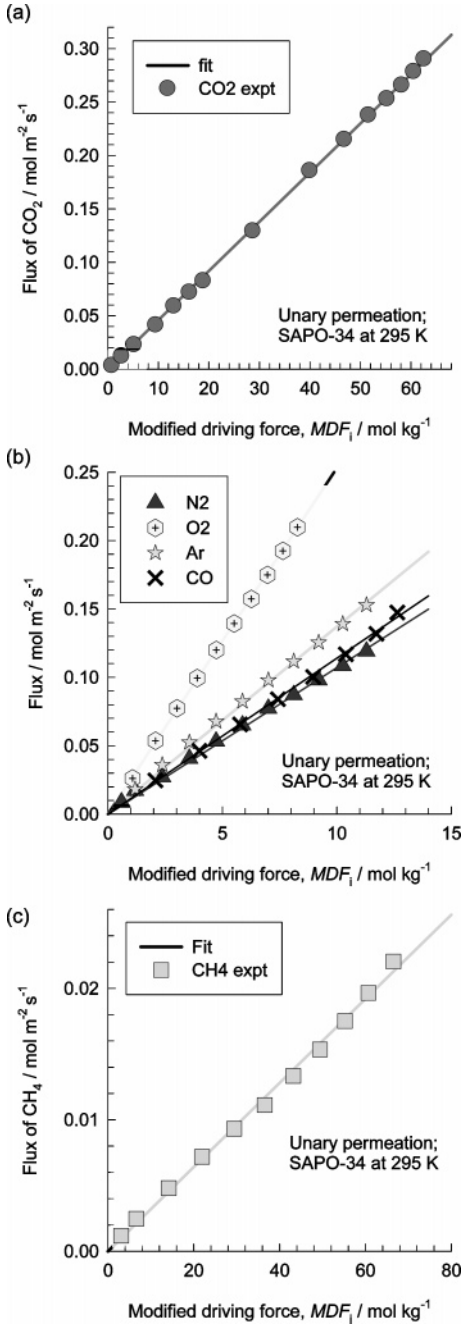

Figure 5. The experimental data on unary permeation fluxes of (a) CO_2, (b) N_2, CO, O_2, Ar and (c) CH_4 is plotted against the modified driving force MDF_i, calculated from eq 12, taking the parameter values specified in Table 2. The straight lines are drawn using eq 13 with fitted values of $\rho Đ_i(0)/\delta$ specified in Table 2.

dependencies of N_i on MDF_i are listed in Table 2 along with the corresponding zero-loading transport coefficients $\rho Đ_i(0)/\delta$.

To rationalize the values of the zero-loading transport diffusivities and Reed−Ehrlich parameter ϕ_i, we need information on the molecular dimensions. Figure 6 presents drawings showing approximate molecular dimensions of the various gases used in these investigations; these dimensions were estimated using published force fields for molecule−molecule interactions.[30−32] The values of the zero-loading transport coefficients $\rho Đ_i(0)/\delta$ appear to decrease sharply as the molecular diameter approaches the window size, which has a value of 3.8 Å for SAPO-34; see Figure 7a. For CO_2, N_2, CO, and Ar, the molecular diameter is in the 3−3.4 Å range and the $\rho Đ_i(0)/\delta$ appear to decrease with increasing molecular length; see Figure 7b. The loading-

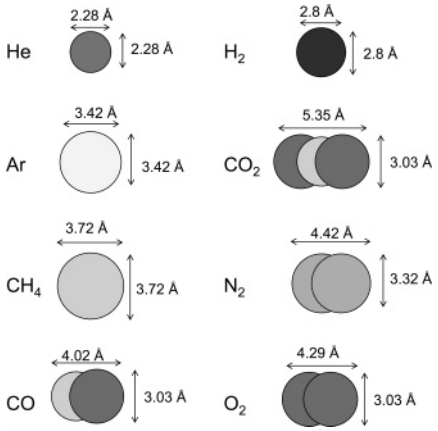

Figure 6. Drawing showing the approximate molecular dimensions of He, H_2, CO_2, N_2, O_2, CO, Ar, and CH_4.

TABLE 2: Reed−Ehrlich Parameters in Various Zeolite Structures

		Reed-Ehrlich model parameters in eqs 10 and 11	
molecule	$\rho Đ_i(0)/\delta$	z	ϕ_i
He	0.322		
H_2	0.293		
CO_2	4.6×10^{-3}	5	2.1
CH_4	3.2×10^{-4}	5	3
N_2	1.07×10^{-2}	5	2.3
O_2	2.53×10^{-2}	5	1.8
CO	1.14×10^{-2}	5	2
Ar	1.37×10^{-2}	5	2

dependence is stronger when the molecular diameter is larger; see Figure 7c. For an interpretation of the loading-dependence of the M-S diffusivity in terms of the free energy barrier for hopping of molecules between cages, see the papers of Beerdsen et al.[18,33]

4. Modeling of Mixture Permeation

The M-S equations[13,34,35]

$$-\rho\frac{q_i}{RT}\frac{\mathrm{d}\mu_i}{\mathrm{d}x}=\sum_{\substack{j=1\\ j\neq 1}}^{n}\frac{q_jN_i-q_iN_j}{q_{j,\mathrm{sat}}Đ_{ij}}+\frac{N_i}{Đ_i};\quad i=1,...n \qquad (14)$$

are widely used for modeling and interpretation of zeolite membrane permeation experiments for a variety of molecules and mixtures.[3,36,37] In eq 14, $Đ_i$ is the M-S diffusivity of species i in the mixture, q_i is the molar loading, $q_{i,\mathrm{sat}}$ is the saturation capacity of species i, $Đ_{ij}$ are the binary exchange coefficients. The major advantage of using the M-S equations is that the diffusion coefficients $Đ_i$ and $Đ_{ij}$ can be estimated from pure component adsorption and diffusion data.[13,35] Zhu et al.[38] and Li et al.[23] have modeled permeation of CO_2 (1)−CH_4 (2) mixtures across MFI and SAPO-34 membranes, respectively by estimating that the binary exchange parameter $Đ_{ij}$ using the interpolation formula.

$$Đ_{ij}=[Đ_i]^{q_i/(q_i+q_j)}\,[Đ_j]^{q_j/(q_i+q_j)} \qquad (15)$$

On the basis of MD simulations of diffusion in CO_2−CH_4 mixtures, Krishna et al.[21,32] have argued that in zeolite structures that consist of cages separated by narrow windows, such as CHA and DDR, intercage jumps are uncorrelated and that as an approximation, the binary exchange coefficient $Đ_{12}$ can be taken to be infinite, that is

$$N_i=-\rho Đ_i\frac{q_i}{RT}\frac{\mathrm{d}\mu_i}{\mathrm{d}x};\quad i=1,...n \qquad (16)$$

SAPO-34 is an isotype of CHA and the same approximation may be expected to hold. The gradient of the chemical potentials in eq 16 can be related to the gradients in the loadings by defining a matrix of thermodynamic factors [Γ]

$$\frac{q_i}{RT}\frac{\mathrm{d}\mu_i}{\mathrm{d}x}=\sum_{j=1}^{n}\Gamma_{ij}\frac{\mathrm{d}q_j}{\mathrm{d}x};\quad \Gamma_{ij}\equiv\frac{q_i}{f_i}\frac{\partial f_i}{\partial q_j};\quad i,j=1,..2 \qquad (17)$$

The elements Γ_{ij} in eq 17 can be estimated using the ideal-adsorbed solution theory of Myers and Prausnitz[39] and the fits

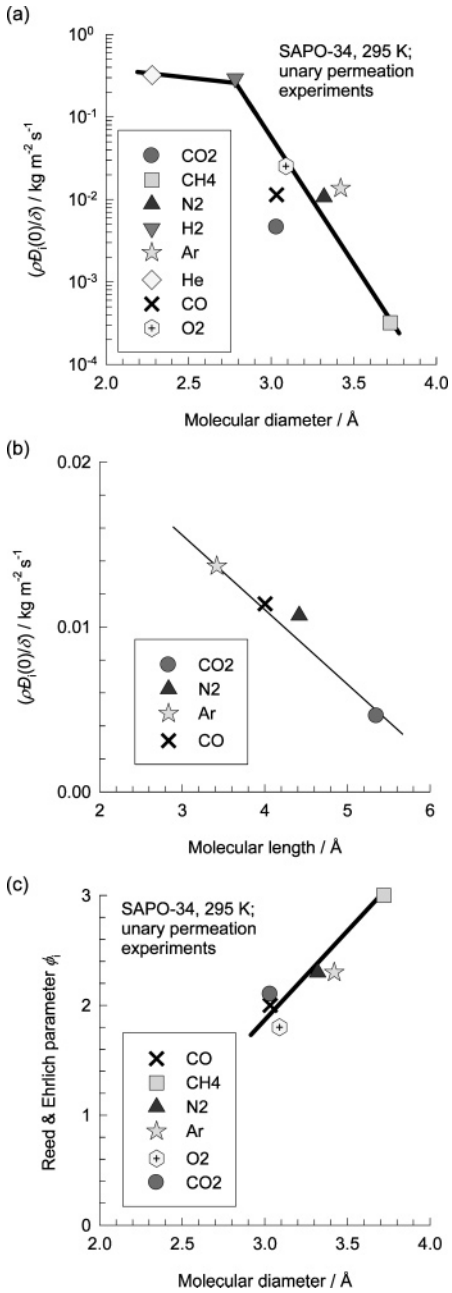

Figure 7. Dependence of (a) the zero-loading transport coefficient $\rho Đ_i(0)/\delta$ on the molecular diameter, (b) the zero-loading transport coefficient $\rho Đ_i(0)/\delta$ on the molecular length, and (c) the Reed−Ehrlich parameter ϕ_i on the molecular diameter.

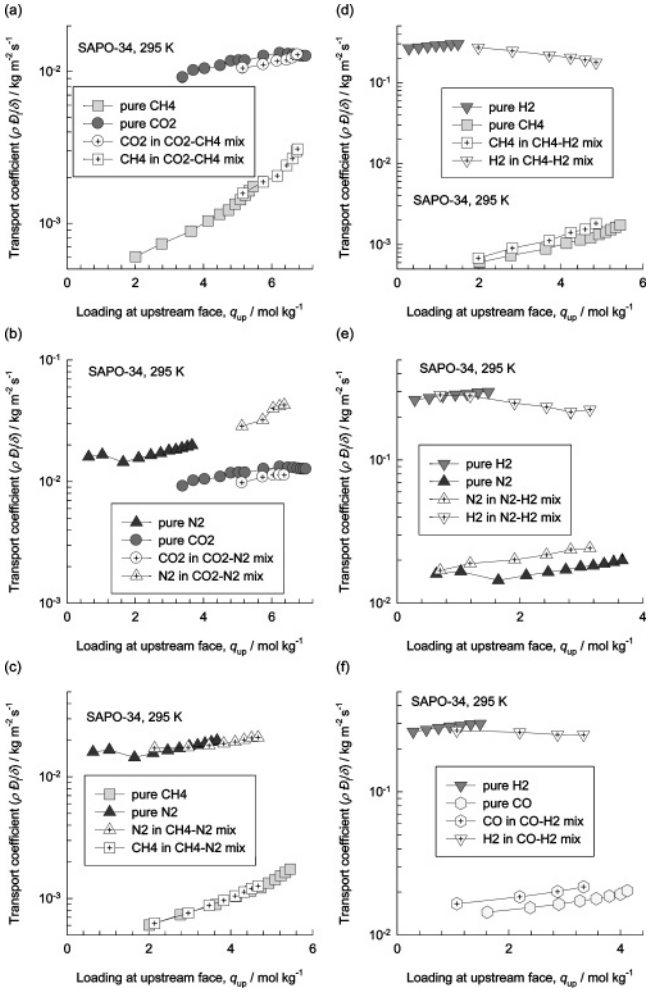

Figure 8. Comparison of transport coefficients, $\rho Đ_i/\delta$, backed out from unary permeation and binary mixtures containing (a) CO_2/CH_4, (b) CO_2/N_2, (c) N_2/CH_4, (d) CH_4/H_2, (e) N_2/H_2, and (f) CO/H_2.

of the pure component isotherms. Integrating eq 17 across the membrane thickness we obtain

$$N_i = \frac{\rho}{\delta}\int_{\text{upstream}}^{\text{downstream}} Đ_i \sum_{j=1}^{n}\left(\Gamma_{ij}\frac{\mathrm{d}q_j}{\mathrm{d}x}\right)\mathrm{d}x; \quad i = 1,...n \quad (18)$$

The details of the numerical procedures for calculation of the fluxes are described in earlier work.[3,40]

Before proceeding with the estimation of the fluxes N_i using the pure component data on the transport coefficients listed in Table 2, we shall demonstrate the applicability of the uncoupled M-S equations (18) by backing out the transport diffusivity $\rho Đ_i/\delta$ as a function of the total upstream loading, $q_{up} = q_{1,up} + q_{2,up}$, for the six binary mixture permeation experiments using

$$\frac{\rho Đ_i}{\delta} = \frac{N_i}{\int_{\text{upstream}}^{\text{downstream}} \sum_{j=1}^{n}\left(\Gamma_{ij}\frac{\mathrm{d}q_j}{\mathrm{d}x}\right)\mathrm{d}x}; \quad i = 1,...n \quad (19)$$

The results are presented in Figure 8a−f, along with the backed-out transport coefficients from unary permeation experiments (reported in Figure 4a,b). For the (a) CO_2/CH_4, (b) CO_2/N_2, and (c) CH_4/N_2 mixtures, we note that the $\rho Đ_i/\delta$ backed out either from pure component or mixture permeation experiments exhibit similar loading-dependences and correspond closely to each other. This confirms that the assumption of

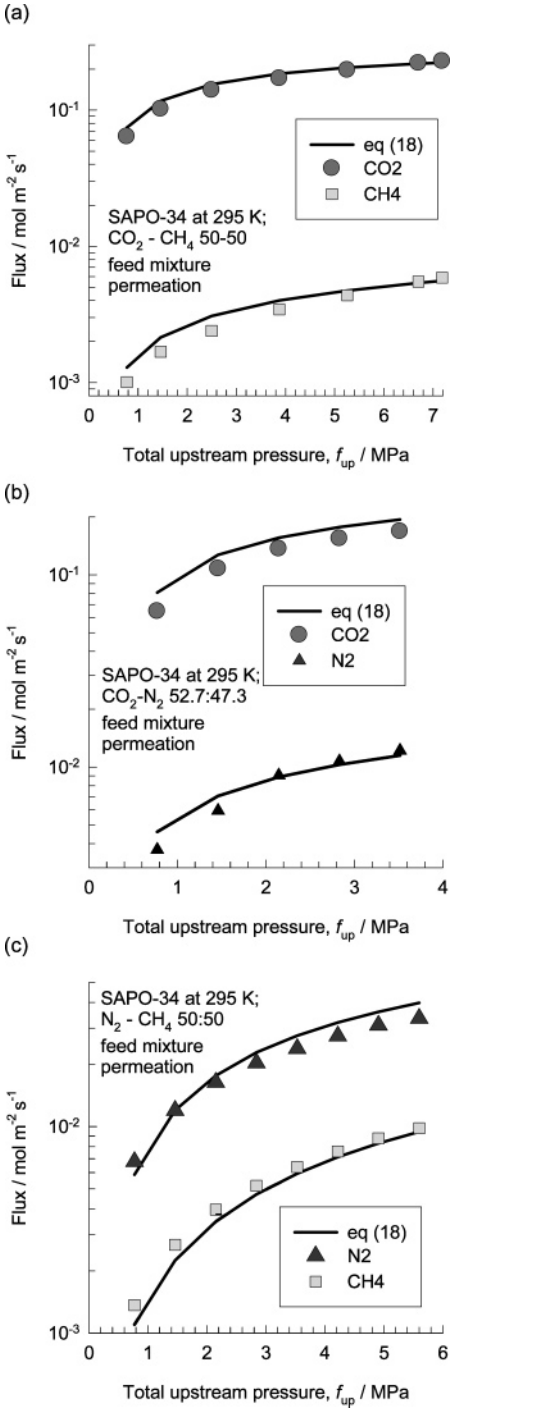

Figure 9. Permeation fluxes for binary (a) CO_2/CH_4, (b) CO_2/N_2, and (c) N_2/CH_4 mixtures as function of the upstream total pressure, f_{up}. The continuous solid lines represent the calculations by numerical solution of eq 18.

infinite value for the binary exchange parameter $Đ_{12}$ is a good one. A slightly different picture emerges for the mixture containing H_2. From the $\rho Đ_i/\delta$ data for CH_4/H_2, N_2/H_2, and CO/H_2 mixtures (see Figure 8d−f), there appears to be a slight slowing-down of the more mobile H_2 with a concomitant and small speeding-up of the more tardy species, CH_4, N_2, and CO in the three binary mixtures, respectively. This would indicate that the assumption of an infinite value of $Đ_{12}$ is not as good for mixtures with hydrogen and must be viewed only as an approximation.

It now remains to compare the estimate of the permeation fluxes in the mixture from eq 18 with experimental values. The

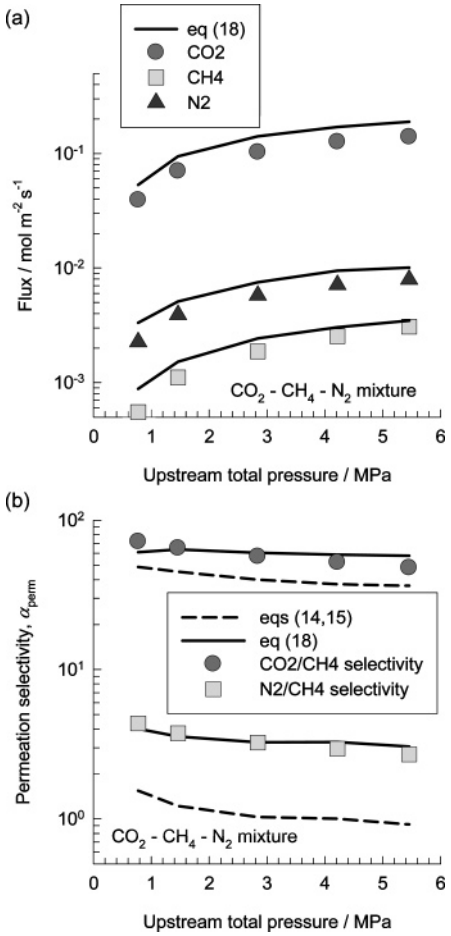

Figure 10. (a) Permeation fluxes and (b) permeation selectivities α_{perm}, for ternary $CO_2/CH_4/N_2$ mixture as a function of the upstream total pressure, f_{up}. The continuous solid lines represent the calculations by the numerical solution of eq 18 across the membrane. The dashed lines represent integration of eqs 14 and 15 across the membrane.

M-S diffusivity $Đ_i$ of component i in the mixture is estimated on the basis of the total mixture occupancy, θ, defined by

$$\theta = \sum_{i=1}^{n} \frac{q_i}{q_{i,\text{sat}}} \tag{20}$$

and the Reed−Ehrlich model, eq 10, and the pure component transport data in Table 2. Figure 9a−c shows that the estimations of N_i using eq 18 for (a) CO_2/CH_4, (b) CO_2/N_2, and (c) CH_4/N_2 mixtures are in very good agreement with experimental values (filled solid symbols) for the entire range of upstream pressure conditions. This result is to be expected in view of the good agreement in the backed-out transport coefficients $\rho Đ_i/\delta$ of mixtures with that of pure component data; cf. Figure 8a−c.

Figure 10a shows the experimentally determined fluxes for the ternary $CO_2/CH_4/N_2$ mixture as a function of the upstream total pressure. The predictions of the M-S mixture model (eq 18), shown by the continuous solid lines in Figure 10a, are in good agreement with experiment. Figure 10b shows the experimentally determined permeation selectivity α_{perm} defined by

$$\alpha_{perm} = \frac{N_1/N_2}{f_{1,up}/f_{2,up}} \tag{21}$$

for CO_2/CH_4 and N_2/CH_4 separation in the ternary mixture. Inclusion of the binary exchange coefficients $Đ_{ij}$, estimated

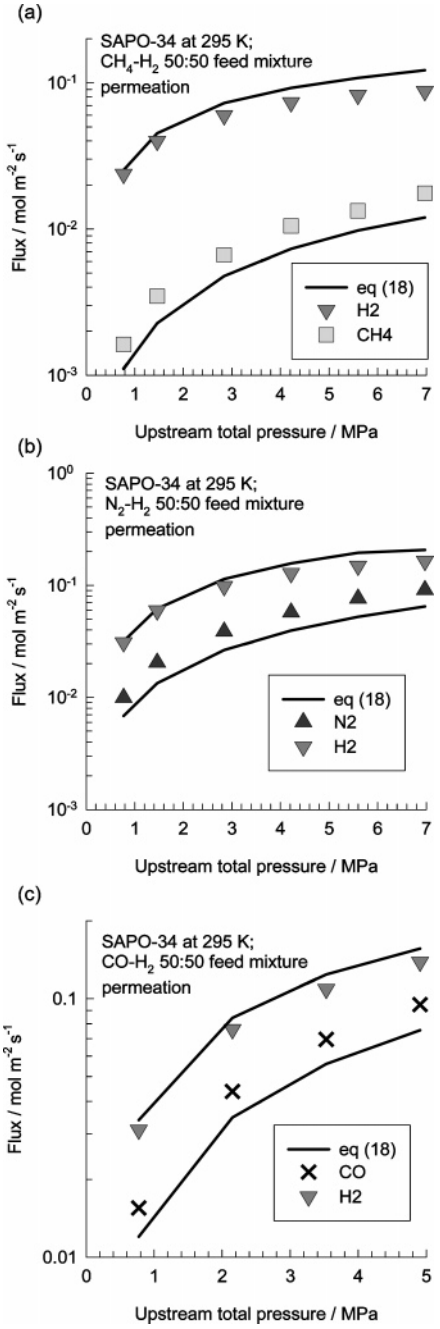

Figure 11. Permeation fluxes for binary (a) CH_4/H_2, (b) N_2/H_2, and (c) CO/H_2 mixtures as function of the upstream total pressure, f_{up}. The continuous solid lines represent the calculations by numerical solution of eq 18 across the membrane.

using eq 15 in the M-S equation (14), will have the effect of slowing-down the "faster" molecules, while concomitantly speeding-up the "tardier" molecules. These predictions are shown by the dashed lines in Figure 10b; for both mixtures this leads to a significantly poorer match with experiments. For CO_2/CH_4 and N_2/CH_4 mixtures, allowance for a finite binary exchange coefficient $Đ_{ij}$ predicts a significantly lower α_{perm} than in the experiments because in both these cases we have slowing-down of the more mobile CO_2, or N_2, and concomitant speeding-up of the tardy CH_4. The conclusion to be drawn from the results presented in Figure 10b is that intercage hopping of molecules CO_2, CH_4, and N_2 within SAPO-34 occurs independent of one other and validates the use of the simplified M-S equation (18). There is no perceptible slowing-down or speeding-up process. The window size of SAPO-34 is of the order of 3.8 Å, and

only one molecule can pass through the window at a time. The intercage hopping of molecules between cages is uncorrelated, and the three binary exchange coefficients $Đ_{ij}$ all have large values.

We now turn to permeation of the mixture containing H_2; the measured fluxes for binary (a) CH_4/H_2, (b) N_2/H_2, and (c) CO/H_2 mixtures with equimolar feed mixture compositions are shown in Figure 11a−c (filled solid symbols) as a function of the total upstream pressure, f_{up}. The model calculations are indicated by continuous solid lines in Figure 11. For all three binary mixtures, the fluxes are predicted with reasonable accuracy using only pure component diffusivity and isotherm data. We note, however, that for all three mixtures the fluxes of H_2 are slightly overestimated; the reason for this is that there is a slight slowing-down of H_2 in the mixture due to the presence of the tardy companion species (CH_4, N_2, or CO) as was stressed earlier; cf. Figure 8d−f. We see also note that the estimation of the fluxes of CH_4, N_2, and CO are slightly lower than found experimentally; this is due to the slight speeding-up of these tardier components. The assumption of infinite exchange $Đ_{12}$ is to be considered as a reasonable, but not perfect, approximation for hydrogen containing mixtures.

5. Conclusions

The following conclusions can be drawn from the results presented in this paper.

(1) The M-S diffusivities $Đ_i$ of He, H_2, CO_2, N_2, O_2, CO, Ar, and CH_4 in SAPO-34 have been backed out using unary permeation data. While the assumption of a loading-independent $Đ_i$ is valid for He and H_2, the M-S diffusivities of CO_2, N_2, O_2, CO, Ar, and CH_4 are all significantly loading-dependent.

(2) The model of Reed−Ehrlich provides a convenient practical procedure for modeling the loading-dependence of $Đ_i$; the severity of the loading-dependence is captured in this model by the parameter ϕ_i. The larger the diameter is of the molecule, the stronger the loading-dependence is.

(3) Binary CO_2/CH_4, CO_2/N_2, CH_4/N_2, and ternary $CO_2/CH_4/N_2$ mixture permeation in SAPO-34 is best modeled by the M-S equation (18) wherein the intercage hopping of molecules is taken to be independent of one another. This corresponds with the assumption of an infinite exchange coefficient $Đ_{ij}$.

(4) For permeation of binary mixtures H_2/CH_4, H_2/N_2, and H_2/CO, the assumption of infinite exchange coefficient $Đ_{12}$ is not a perfect one; there is a slight slowing-down of mobile H_2 with concomitant speeding-up of the tardier CH_4, N_2, or CO. Even so, the estimations of the fluxes using eq 18 are in reasonably good agreement with experiment.

Acknowledgment. The Boulder group gratefully acknowledges support by the National Science Foundation, CTS-0413027, and Shell Global Solutions. R.K. acknowledges the grant of a TOP subsidy from The Netherlands Foundation for Fundamental Research (NWO−CW) for intensification of reactors. Dr. J.M. van Baten provided valuable assistance with GCMC simulations of the He isotherm.

Supporting Information Available: This includes details of membrane synthesis, characterization, and measurement procedures along with the experimental data. This material is available free of charge via the Internet at http://pubs.acs.org/.

References and Notes

(1) Davis, M. E. *Nature* **2002**, *417*, 813−821.
(2) Davis, M. E. *Science* **2003**, *300*, 438−439.
(3) Krishna, R.; Baur, R. *Sep. Purif. Technol.* **2003**, *33*, 213−254.
(4) Sholl, D. S.; Johnson, J. K. *Science* **2006**, *312 (5776)*, 1003−1004.
(5) Snurr, R. Q.; Hupp, J. T.; Nguyen, S. T. *AIChE J.* **2004**, *50*, 1090−1095.
(6) Kärger, J.; Ruthven, D. M. *Diffusion in Zeolites and Other Microporous Solids*; John Wiley: New York, 1992.
(7) Jobic, H.; Kärger, J.; Bée, M. *Phys. Rev. Lett.* **1999**, *82*, 4260−4263.
(8) Chong, S. S.; Jobic, H.; Plazanet, M.; Sholl, D. S. *Chem. Phys. Lett.* **2005**, *408*, 157−161.
(9) Jobic, H.; Laloué, C.; Laroche, C.; van Baten, J. M.; Krishna, R. *J. Phys. Chem. B* **2006**, *110*, 2195−2201.
(10) Papadopoulos, G. K.; Jobic, H.; Theodorou, D. N. *J. Phys. Chem. B* **2004**, *108*, 12748−12756.
(11) Skoulidas, A. I.; Sholl, D. S. *J. Phys. Chem. A* **2003**, *107*, 10132−10141.
(12) Chempath, S.; Krishna, R.; Snurr, R. Q. *J. Phys. Chem. B* **2004**, *108*, 13481−13491.
(13) Krishna, R.; van Baten, J. M. *J. Phys. Chem. B* **2005**, *109*, 6386−6396.
(14) Krishna, R.; van Baten, J. M. *Chem. Phys. Lett.* **2005**, *407*, 159−165.
(15) Krishna, R.; van Baten, J. M. *J. Phys. Chem. B* **2006**, *110*, 2195−2201.
(16) van Baten, J. M.; Krishna, R. *Microporous Mesoporous Mater.* **2005**, *84*, 179−191.
(17) Beerdsen, E.; Dubbeldam, D.; Smit, B. *Phys. Rev. Lett.* **2005**, *93*, 248301.
(18) Beerdsen, E.; Dubbeldam, D.; Smit, B. *Phys. Rev. Lett.* **2006**, *96*, 044501.
(19) Beerdsen, E.; Smit, B. *J. Phys. Chem. B* **2006**, *110*, 14529−14530.
(20) Krishna, R.; van Baten, J. M. *Chem. Eng. Technol.* **2006**, *29*, 1429−1437.
(21) Krishna, R.; van Baten, J. M.; García-Pérez, E.; Calero, S. *Ind. Eng. Chem. Res.* [Online early access]. DOI: 10.1021/ie060693d. 2007
(22) Reed, D. A.; Ehrlich, G. *Surf. Sci.* **1981**, *102*, 588−609.
(23) Li, S.; Martinek, J. G.; Falconer, J. L.; Noble, R. D.; Gardner, T. Q. *Ind. Eng. Chem. Res.* **2005**, *44*, 3220−3228.
(24) Li, S.; Falconer, J. L.; Noble, R. D.; Krishna, R. *Ind. Eng. Chem. Res.* [Online early access]. DOI: 10.1021/ie0610703. 2007
(25) Ruthven, D. M. *Principles of Adsorption and Adsorption Processes*; John Wiley: New York, 1984.
(26) Mäder, U. K.; Berman, R. G. *Am. Mineral.* **1991**, *76*, 1547−1559.
(27) Golden, T. C.; Sircar, S. *J. Colloid Interface Sci.* **1994**, *162*, 182−188.
(28) Skoulidas, A. I.; Sholl, D. S. *J. Phys. Chem. B* **2002**, *106*, 5058−5067.
(29) Krishna, R.; Paschek, D.; Baur, R. *Microporous Mesoporous Mater.* **2004**, *76*, 233−246.
(30) Dubbeldam, D.; Calero, S.; Vlugt, T. J. H.; Krishna, R.; Maesen, T. L. M.; Smit, B. *J. Phys. Chem. B* **2004**, *108*, 12301−12313.
(31) Makrodimitris, K.; Papadopoulos, G. K.; Theodorou, D. N. *J. Phys. Chem. B* **2001**, *105*, 777−788.
(32) Krishna, R.; van Baten, J. M.; García-Pérez, E.; Calero, S. *Chem. Phys. Lett.* **2006**, *429*, 219−224.
(33) Beerdsen, E.; Dubbeldam, D.; Smit, B. *Phys. Rev. Lett.* **2005**, *95*, 164505.
(34) Kapteijn, F.; Moulijn, J. A.; Krishna, R. *Chem. Eng. Sci.* **2000**, *55*, 2923−2930.
(35) Krishna, R.; van Baten, J. M. *Ind. Eng. Chem. Res.* **2006**, *45*, 2084−2093.
(36) van de Graaf, J. M.; Kapteijn, F.; Moulijn, J. A. *AIChE J.* **1999**, *45*, 497−511.
(37) Millot, B.; Methivier, A.; Jobic, H.; Moueddeb, H.; Bee, M. *J. Phys. Chem. B* **1999**, *103*, 1096−1101.
(38) Zhu, W.; Hrabanek, P.; Gora, L.; Kapteijn, F.; Moulijn, J. A. *Ind. Eng. Chem. Res.* **2006**, *45*, 767−776.
(39) Myers, A. L.; Prausnitz, J. M. *AIChE J.* **1965**, *11*, 121−130.
(40) Krishna, R.; Baur, R. Diffusion, Adsorption, and Reaction in Zeolites: Modelling and Numerical Issues. http://www.science.uva.nl/research/cr/zeolite/, University of Amsterdam (accessed November 11, 2004).

Supporting information to accompany:

Interpreting unary, binary and ternary mixture permeation across SAPO-34 membrane with loading dependent Maxwell-Stefan diffusivities

Shiguang Li[(1)], John L. Falconer[(1)], Richard D. Noble[(1)], and R. Krishna[(2)]*

[(1)] Department of Chemical and Biological Engineering, University of Colorado

Boulder, CO 80309-0424, U.S.A.

[(2)]Van 't Hoff Institute for Molecular Sciences, University of Amsterdam, Nieuwe Achtergracht 166,

1018 WV Amsterdam, The Netherlands.

Experimental Methods and Data

1. Experimental Methods

Membrane Synthesis

SAPO-34 membranes were synthesized by seeding on porous stainless steel tubes (0.8-μm pores, Pall Corp.). The detailed synthesis procedure was given elsewhere.[1] Non-porous, stainless steel tubes were welded onto each end of supports. The permeate area was approximately 7.8 cm^2. The synthesis gel composition for SAPO-34 seeds was 1.0 Al_2O_3 : 1.0 P_2O_5 : 0.3 SiO_2 : 1.2 TEAOH : 55 H_2O. This composition is different to that used in our previous published study.[2]

The gel was prepared by stirring H_3PO_4 (85 wt% aqueous solution, Aldrich), Al(i-$C_3H_7O)_3$ (> 99.99%, Aldrich), and distilled H_2O at room temperature for 12 h. Then the template, tetra-ethyl ammonium hydroxide (TEAOH, 35 wt% aqueous solution, Aldrich), was added and the mixture stirred for 30 min before the colloidal silica sol (Ludox AS40, 40% aqueous solution, Aldrich) was added to the mixture. The solution was sealed, stirred, and aged for approximately 24 h at room temperature. Next, the gel was added to a Teflon-lined autoclave. The hydrothermal synthesis was carried at 493 K for about 24 h. After synthesis, the powder was collected and washed with distilled water at 295 K for three times, and then dried at 373 K in a vacuum oven for 2 h. The powder was calcined at 823 K for 10 h. The heating and cooling rates were 6 K/min. The calcined crystals were used as seeds for membrane preparation.

Before membrane synthesis, the supports were boiled in distilled water for 3 h and dried at 373 K under vacuum for 30 min. The stainless steel tubes were then wrapped with Teflon tape on their outside. The tubes were then treated by rubbing the inside surface of the support tube with dry SAPO-34 particles. The seeded tubes were placed in an autoclave, which was then filled with the synthesis gel that has the same composition as that used for seeds. The hydrothermal synthesis was carried at 493 K for about 24 h. After synthesis, the membrane was washed with distilled water at 295 K and dried at 373 K in a vacuum oven for 2 h. A second synthesis step was applied using the same procedure, but the tube

was inverted to obtain a more uniform layer. The membranes were calcined in air at 663 K for 10 h. The heating and cooling rates were 0.6 and 0.9 K/min, respectively.

Characterization

Crystals collected during membrane synthesis were calcined at 823 K for 10 h, and then used in various analyses including adsorption measurements. X-ray diffraction (XRD, Scintag PAD-V diffractometer) confirmed the CHA structure. The chemical composition of the crystals determined by inductively coupled plasma analysis (Varian UltraMass 700 inductively coupled plasma mass spectrometer with a CETAC LXS-200+ laser ablation system) was $(Si_{0.061}Al_{0.483}P_{0.455})O_2$.

Adsorption experiments were carried out in an Autosorb-1 (Quantachrome Corp. Model AS1-C-VP-RGA) system. Prior to each adsorption experiment, the sample was outgassed in vacuum at 493 K for at least 2 h. Adsorption isotherms for H_2, CO_2, CH_4 , N_2, O_2, Ar, and CO were measured at 295 K.

Nitrogen adsorption was performed at 77 K to determine the BET surface area and micropore volume. The SAPO-34 zeolite had a BET surface area of 500 m^2/g and a micropore volume of 0.26 cm^3/g.

Permeation experiments

Unary, binary and ternary mixture permeations were measured in the flow system described previously;[2] the system was modified to operate up to 7.2 MPa pressure. The membrane was mounted in a stainless steel module and sealed at each end with silicone o-rings. The pressure on each side of the membrane was independently controlled. Unary and mixture permeations were investigated as functions of feed pressure while maintaining a constant permeate pressure of 84 kPa. Fluxes were measured using a soap film bubble flow meter. The system was leak checked by replacing the membrane with a solid stainless steel tube. The leak rate for a 7-MPa pressure drop across the O-ring was less than 0.01% of the measured CH_4 flux for a 50/50 mixture at the same pressure drop across a membrane.

Figure 1 shows a schematic of the membrane set-up.The compositions of the feed, retentate, and permeate streams were measured online using a SRI 8610 C GC gas chromatograph equipped with a thermal conductivity detector and HAYESEP-D column (Alltech). The oven, injector, and detector temperatures were all kept at 423 K.

2. Permeation data

The experimental data for unary permeation of CO_2 CH_4, N_2, He, H_2, O_2, CO and He are presented in Tables 1, 2 3, 4, 5, 6, 7, and 8. The binary permeation data N_2/H_2, CH_4/H_2 and CO/H_2 mixtures are presented in Tables 9, 10 and 11. The binary permeation data for CO_2/CH_4, CO_2/N_2, and N_2/CH_4 mixtures are summarized in Tables 12, 13, and 14. The ternary permeation data for $CO_2/N_2/CH_4$ mixtures are presented in Table 15. The gas phase compositions of the retentate (upstream) and permeate (downstream) compartments were also measured and on this basis the partial pressures on both compartments were determined. The *average* (logarithmic mean) values of the upstream partial pressures, $f_{i,up}$, are reported in Tables 9, 10, 11, 12, 13, 14, and 15 were used. For purposes of model calculations to compare with experiments, these precise partial pressures as specified in the second and third columns of Tables 9, 10, 9, 10, 11, 12, 13, 14, and 15 were used.

For plotting purposes the total upstream pressures, listed in the first column in Tables 9, 10, 11, 12, 13, 14, and 15 are employed on the x-axis in the main text of this paper.

3. Literature cited

(1) Li, S.; Falconer, J. L.; Noble, R. D. *Adv. Mater.* **2006**, *16*, 2601-2603.
(2) Li, S.; Martinek, J. G.; Falconer, J. L.; Noble, R. D.; Gardner, T. Q. *Ind. Eng. Chem. Res.* **2005**, *44*, 3220-3228.

Table 1. Unary CO_2 permeation data.

Upstream pressure, $f_{i,up}$	Downstream pressure, $f_{i,down}$	CO_2 flux, N_i
0.094	0.084	0.0033
0.118	0.084	0.0122
0.153	0.084	0.0228
0.222	0.084	0.0412
0.291	0.084	0.0589
0.360	0.084	0.0719
0.429	0.084	0.0825
0.773	0.084	0.1293
1.463	0.084	0.1857
2.152	0.084	0.2150
2.842	0.084	0.2377
3.531	0.084	0.2531
4.221	0.084	0.2657
4.910	0.084	0.2784
5.600	0.084	0.2903

$f_{i,up}$ and $f_{i,down}$ have the units MPa, N_i are expressed in mol m^{-2} s^{-1}

Table 2. Unary CH_4 permeation data.

Upstream pressure, $f_{i,up}$	Downstream pressure, $f_{i,down}$	CH_4 flux, N_i
0.43	0.084	0.0012
0.77	0.084	0.0025
1.46	0.084	0.0048
2.15	0.084	0.0072
2.84	0.084	0.0093
3.53	0.084	0.0111
4.22	0.084	0.0133
4.91	0.084	0.0154
5.60	0.084	0.0175
6.29	0.084	0.0197
7.08	0.084	0.0220

$f_{i,up}$ and $f_{i,down}$ have the units MPa, N_i are expressed in mol m^{-2} s^{-1}

Table 3. Unary N_2 permeation data.

Upstream pressure, $f_{i,up}$	Downstream pressure, $f_{i,down}$	N_2 flux, N_i
0.43	0.084	0.009
0.77	0.084	0.017
1.46	0.084	0.027
2.15	0.084	0.041
2.84	0.084	0.053
3.53	0.084	0.065
4.22	0.084	0.077
4.91	0.084	0.087
5.60	0.084	0.098
6.29	0.084	0.108
6.98	0.084	0.119

$f_{i,up}$ and $f_{i,down}$ have the units MPa, N_i are expressed in mol m^{-2} s^{-1}

Table 4. Unary He permeation data.

Upstream pressure, $f_{i,up}$	Downstream pressure, $f_{i,down}$	He flux, N_i
0.43	0.084	0.0293
0.77	0.084	0.0586
1.46	0.084	0.0898
2.15	0.084	0.1226
2.84	0.084	0.1517
3.53	0.084	0.1822
4.22	0.084	0.2168
4.91	0.084	0.2446
5.60	0.084	0.2730
6.29	0.084	0.3013
6.98	0.084	0.0293

$f_{i,up}$ and $f_{i,down}$ have the units MPa, N_i are expressed in mol m^{-2} s^{-1}

Table 5. Unary H_2 permeation data.

Upstream pressure, $f_{i,up}$	Downstream pressure, $f_{i,down}$	H_2 flux, N_i
0.77	0.084	0.0688
1.46	0.084	0.1394
2.15	0.084	0.2114
2.84	0.084	0.2839
3.53	0.084	0.3524
4.22	0.084	0.4263
4.91	0.084	0.4926

$f_{i,up}$ and $f_{i,down}$ have the units MPa, N_i are expressed in mol m^{-2} s^{-1}

Table 6. Unary O_2 permeation data.

Upstream pressure, $f_{i,up}$	Downstream pressure, $f_{i,down}$	O_2 flux, N_i
0.77	0.084	0.0261
1.46	0.084	0.0536
2.15	0.084	0.0773
2.84	0.084	0.0995
3.53	0.084	0.1200
4.22	0.084	0.1394
4.91	0.084	0.1574
5.60	0.084	0.1749
6.29	0.084	0.1924
6.98	0.084	0.2097

$f_{i,up}$ and $f_{i,down}$ have the units MPa, N_i are expressed in mol m^{-2} s^{-1}

Table 7. Unary CO permeation data.

Upstream pressure, $f_{i,up}$	Downstream pressure, $f_{i,down}$	CO flux, N_i
0.77	0.084	0.0246
1.46	0.084	0.0462
2.15	0.084	0.0655
2.84	0.084	0.0840
3.53	0.084	0.1002
4.22	0.084	0.1168
4.91	0.084	0.1319
5.41	0.084	0.1473

$f_{i,up}$ and $f_{i,down}$ have the units MPa, N_i are expressed in mol m^{-2} s^{-1}

Table 8. Unary Ar permeation data.

Upstream pressure, $f_{i,up}$	Downstream pressure, $f_{i,down}$	Ar flux, N_i
0.77	0.084	0.0182
1.46	0.084	0.0359
2.15	0.084	0.0524
2.84	0.084	0.0678
3.53	0.084	0.0824
4.22	0.084	0.0980
4.91	0.084	0.1117
5.60	0.084	0.1255
6.29	0.084	0.1392
6.98	0.084	0.1529

$f_{i,up}$ and $f_{i,down}$ have the units MPa, N_i are expressed in mol m^{-2} s^{-1}

Table 9. Binary N_2-H_2 permeation data

Upstream total pressure f_{up}	N_2 upstream partial pressure $f_{1,up}$	H_2 upstream partial pressure $f_{2,up}$	N_2 downstream partial pressure $f_{1,down}$	H_2 downstream partial pressure $f_{2,down}$	N_2 flux N_1	H_2 flux N_2
0.77	0.39	0.38	0.0204	0.0636	0.0099	0.031
1.46	0.74	0.72	0.0215	0.0625	0.0205	0.060
2.84	1.46	1.38	0.0238	0.0602	0.0387	0.098
4.22	2.19	2.03	0.0260	0.0580	0.0574	0.128
5.60	2.91	2.69	0.0285	0.0555	0.0763	0.149
6.97	3.63	3.35	0.0299	0.0541	0.0911	0.165

$f_{i,up}$ and $f_{i,down}$ have the units MPa, N_i are expressed in mol m^{-2} s^{-1}

Table 10. Binary CH_4 –H_2 permeation data

Upstream total pressure f_{up}	CH_4 upstream partial pressure $f_{1,up}$	H_2 upstream partial pressure $f_{2,up}$	CH_4 downstream partial pressure $f_{1,down}$	H_2 downstream partial pressure $f_{2,down}$	CH_4 flux N_1	H_2 flux N_2
0.77	0.39	0.38	0.0054	0.0786	0.0016	0.024
1.46	0.75	0.71	0.0067	0.0773	0.0035	0.040
2.84	1.47	1.37	0.0084	0.0756	0.0067	0.060
4.22	2.20	2.01	0.0105	0.0735	0.0105	0.073
5.60	2.94	2.66	0.0117	0.0723	0.0133	0.083
6.97	3.67	3.31	0.0140	0.0700	0.0176	0.088

$f_{i,up}$ and $f_{i,down}$ have the units MPa, N_i are expressed in mol m^{-2} s^{-1}

Table 11. Binary CO-H_2 permeation data.

upstream total pressure f_{up}	CO upstream partial pressure $f_{1,up}$	H_2 upstream partial pressure $f_{2,up}$	CO downstream partial pressure $f_{1,down}$	H_2 downstream partial pressure $f_{2,down}$	CO flux N_1	H_2 flux N_2
0.77	0.39	0.38	0.0280	0.0560	0.0155	0.031
2.15	1.10	1.06	0.0307	0.0533	0.0437	0.076
3.53	1.81	1.73	0.0328	0.0512	0.0696	0.109
4.91	2.52	2.39	0.0341	0.0499	0.0948	0.139

$f_{i,up}$ and $f_{i,down}$ have the units MPa, N_i are expressed in mol m^{-2} s^{-1}

Table 12. Binary CO_2-CH_4 permeation data. The feed composition was 50% : 50%.

Total upstream pressure f_{up}	CO_2 upstream partial pressure $f_{1,up}$	CH_4 upstream partial pressure $f_{2,up}$	CO_2 downstream partial pressure $f_{1,down}$	CH_4 downstream partial pressure $f_{2,down}$	CO_2 flux N_1	CH_4 flux N_2
0.77	0.37	0.40	0.083	0.0013	0.064	0.0010
1.46	0.69	0.77	0.083	0.0014	0.102	0.0017
2.50	1.14	1.35	0.083	0.0014	0.140	0.0024
3.88	1.72	2.14	0.082	0.0017	0.171	0.0035
5.26	2.27	2.95	0.082	0.0018	0.196	0.0044
6.70	2.82	3.83	0.082	0.0020	0.221	0.0055
7.19	3.00	4.13	0.082	0.0021	0.228	0.0059

$f_{i,up}$ and $f_{i,down}$ have the units MPa, N_i are expressed in mol m^{-2} s^{-1}

Table 13. Binary CO_2-N_2 permeation data. The feed composition was 52.7% : 47.3%.

Total upstream pressure f_{up}	CO_2 upstream partial pressure $f_{1,up}$	N_2 upstream partial pressure $f_{2,up}$	CO_2 downstream partial pressure $f_{1,down}$	N_2 downstream partial pressure $f_{2,down}$	CO_2 flux N_1	N_2 flux N_2
0.77	0.39	0.38	0.079	0.005	0.065	0.0037
1.46	0.72	0.74	0.080	0.004	0.108	0.0059
2.15	1.04	1.11	0.079	0.005	0.136	0.0091
2.83	1.35	1.48	0.079	0.005	0.154	0.0107
3.52	1.66	1.86	0.078	0.006	0.168	0.0122

$f_{i,up}$ and $f_{i,down}$ have the units MPa, N_i are expressed in mol m^{-2} s^{-1}

Table 14. Binary N_2 –CH_4 permeation data. The feed composition was 50% : 50%.

Total upstream pressure f_{up}	N_2 upstream partial pressure $f_{1,up}$	CH_4 upstream partial pressure $f_{2,up}$	N_2 downstream partial pressure $f_{1,down}$	CH_4 downstream partial pressure $f_{2,down}$	N_2 flux N_1	CH_4 flux N_2
0.773	0.386	0.388	0.079	0.005	0.065	0.0037
1.463	0.728	0.735	0.080	0.004	0.108	0.0059
2.152	1.069	1.084	0.079	0.005	0.136	0.0091
2.842	1.409	1.433	0.079	0.005	0.154	0.0107
3.531	1.748	1.783	0.078	0.006	0.168	0.0122

$f_{i,up}$ and $f_{i,down}$ have the units MPa, N_i are expressed in mol m^{-2} s^{-1}

Table 15. Ternary CO_2 - CH_4 – N_2 permeation data.

Total upstream pressure f_{up}	CO_2 $f_{1,up}$	CH_4 $f_{2,up}$	N_2 $f_{3,up}$	CO_2 $f_{1,down}$	CH_4 $f_{2,down}$	N_2 $f_{3,down}$	CO_2 flux N_1	CH_4 flux N_2	N_2 flux N_3
0.77	0.26	0.26	0.25	0.0784	0.0011	0.0045	0.039	0.0006	0.0023
1.46	0.49	0.50	0.47	0.0784	0.0012	0.0044	0.070	0.0011	0.0039
2.84	0.94	0.98	0.93	0.0782	0.0014	0.0044	0.103	0.0019	0.0058
4.22	1.38	1.45	1.38	0.0780	0.0016	0.0044	0.126	0.0025	0.0072
5.46	1.78	1.88	1.80	0.0778	0.0017	0.0044	0.139	0.0031	0.0079

$f_{i,up}$ and $f_{i,down}$ have the units MPa, N_i are expressed in mol m^{-2} s^{-1}

4. Captions for Figures

Figure 1. Schematic of membrane set-up.